Chem Catalysis

CellPress

Article

Efficient N_2 fixation in air enabled by mechanical-energy-driven triboelectric plasma jet

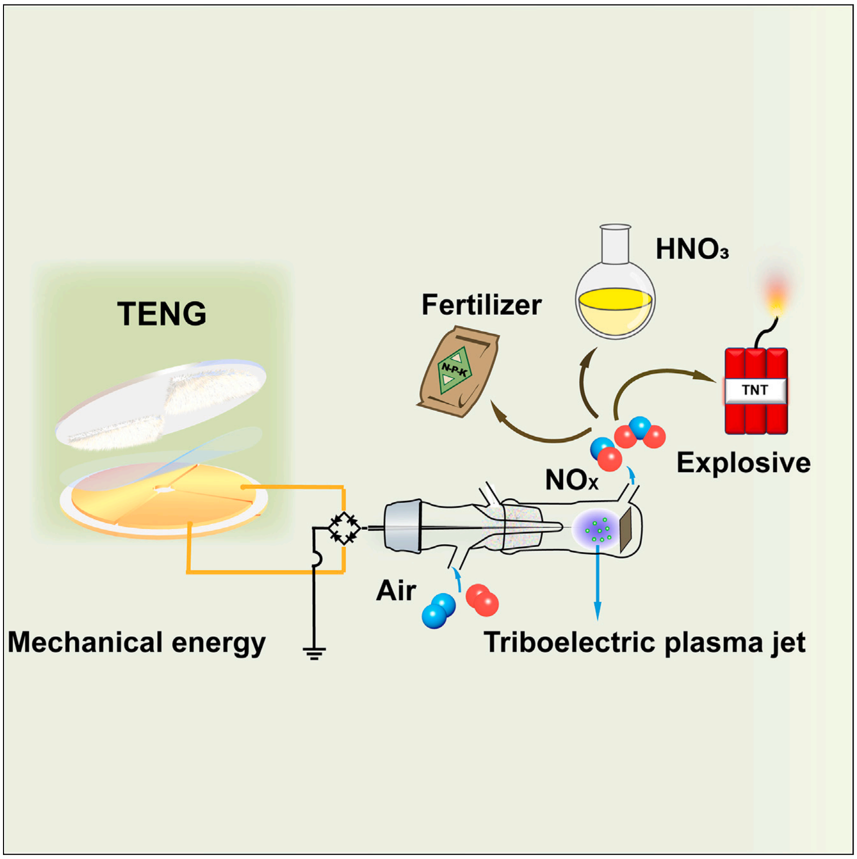

The utilization of mechanical energy and air for N_2 fixation is a promising pathway for production of nitrogen-containing compounds. However, the activity of mechanical energy-driven N_2 fixation systems developed to date is very low. In this work, N_2 fixation with an NOx formation rate of 4.82 μmol h^{-1} and electrical energy cost for NO_X production of 1.76 MJ mol^{-1} N^{-1} was achieved by mechanical-energy-driven triboelectric plasma jet, at conditions of room temperature and atmosphere-pressure air.

7 AFFORDABLE AND CLEAN ENERGY

Jiao Wang, Bao Zhang, Yang Liu, ..., Zhihao Zhang, Gang Cheng, Zuliang Du

zhangbao@henu.edu.cn (B.Z.)
chenggang@henu.edu.cn (G.C.)
zld@henu.edu.cn (Z.D.)

Highlights

Triboelectric plasma jet was constructed to achieve N_2 fixation in air

The achieved NO_X formation rate was 4.82 μmol h^{-1}

The electrical to chemical energy conversion efficiency was 4.92%

The electrical energy cost for NO_X production was 1.76 MJ mol^{-1} N^{-1}

Wang et al., Chem Catalysis *3*, 100647
July 20, 2023 © 2023 Elsevier Inc.
https://doi.org/10.1016/j.checat.2023.100647

Please cite this article in press as: Wang et al., Efficient N_2 fixation in air enabled by mechanical-energy-driven triboelectric plasma jet, Chem Catalysis (2023), https://doi.org/10.1016/j.checat.2023.100647

Chem Catalysis

CellPress

Article

Efficient N_2 fixation in air enabled by mechanical-energy-driven triboelectric plasma jet

Jiao Wang,[1] Bao Zhang,[1,*] Yang Liu,[1] Qinglong Ru,[1] Hongjie Cao,[1] Yifei Zhu,[2] Sumin Li,[1] Zhihao Zhang,[1] Gang Cheng,[1,3,*] and Zuliang Du[1,*]

SUMMARY

N_2 fixation driven by mechanical energy is a promising strategy for production of nitrogen-enriched compounds. However, the activity of mechanical-energy-driven N_2 fixation is very low. Herein, a mechanical-energy-driven triboelectric plasma jet was constructed to achieve N_2 fixation in air at room temperature and atmospheric pressure. Under optimal conditions, the NO_X production rate of 4.82 μmol h^{-1} is 23-fold better than the previous record using a triboelectric nanogenerator. The electrical to chemical energy conversion efficiency and energy cost for NO_X production are 4.92% and 1.76 MJ mol^{-1} N^{-1}, respectively, and the energy cost is the best result in the reported plasma N_2 fixation reaction at room temperature and atmospheric pressure. Because of the lower average energy of electrons in the triboelectric plasma jet, the vibrational excitation dissociation process with low energy barriers is the major mechanism for N_2 fixation. This study provides an effective strategy for N_2 fixation using mechanical energy.

THE BIGGER PICTURE

Artificial N_2 fixation, one of the most important chemical reactions, enables the growth of food for 48% of the global population and has made indelible contributions to the evolution of human civilization. However, the industrial Haber-Bosch process emits large quantities of CO_2, leading to dramatic changes in the global climate. The mechanical-energy-driven triboelectric plasma jet is a potential fossil-fuel-free N_2 fixation process. This study demonstrates that the N_2 fixation process with zero CO_2 emission and direct use of air could be realized using a triboelectric plasma jet driven by mechanical energy. Moreover, this method is a candidate for an efficient, environmentally friendly alternative to the traditional Haber-Bosch process.

INTRODUCTION

N_2 fixation, which converts inert N_2 molecules into active N-containing compounds, is one of the most important chemical reactions in modern industry and is used to synthesize a variety of industrial products, such as fertilizers, drugs, and plastics.[1] Among them, 80% of the N-containing compounds produced in the artificial N_2 fixation process is used to generate fertilizer for crops, feeding nearly 48% of the global population.[2] A large amount of energy is required to dissociate the N_2 molecule owing to its chemical inertness. In the traditional chemical industry, N_2 fixation mainly generates NH_3 through the reaction of N_2 and H_2, which is called the traditional Haber-Bosch (H-B) process.[3] N_2 is generated from the air separation process and H_2 is generated from the natural gas reforming process (Figure 1A).[4] The process is performed under harsh conditions of 450°C–600°C, 200–400 bar, and a high-activity Fe-based catalyst.[5] The H-B process is highly dependent on fossil fuel and is a large-scale industrial process with high energy consumption, CO_2 emissions, and cost. This reaction consumes 1%–2% of the global energy and 2%–3% of global natural gas consumption, and emits up to 3 million tons of CO_2 annually, making it the most energy-consuming industrial process in the chemical industry.[6,7] Large-scale, integrated H-B processes produce N_2-fixed products, which require large amounts of energy to be transported to remote, decentralized crop fertilization sites.[8] These factors seriously limit the H-B process as a decentralized, small-scale, *in situ* N_2 fixation process with low economic input.[9] Therefore, it is vital to develop an economical, environmentally

Please cite this article in press as: Wang et al., Efficient N_2 fixation in air enabled by mechanical-energy-driven triboelectric plasma jet, Chem Catalysis (2023), https://doi.org/10.1016/j.checat.2023.100647

friendly, distributed, and small-scale N_2 fixation chemical industry to replace the traditional H-B technology.[10]

Using renewable energy to drive N_2 immobilization is an ideal strategy to synthesize N-containing compounds. Mechanical energy, including water, wind, tidal, and wave energy, is one of the most common renewable energy sources.[11] It has abundant reserves and numerous sources.[12] However, the intermittency and irregularity of mechanical energy hinders its compatibility with the harsh conditions for traditional and large-scale H-B processes, limiting its applications in N_2 fixation.[13] Triboelectric nanogenerator (TENG) is a recent novel mechanical energy acquisition device that can efficiently convert mechanical into electrical energy, providing a method for the conversion of mechanical into chemical energy.[14] A common strategy is to couple a TENG with electrochemical N_2 reduction reaction devices to form a mechanical-energy-driven electrochemical reduction N_2 system.[15] Due to the mismatch between the high output voltage of TENG and the low voltage of the electrochemical system, low solubility of N_2 in the aqueous solution, and the competitive reaction of hydrogen evolution, the activity of the electrochemical N_2 reduction system driven by the TENG is extremely low (approximately 0.01–0.21 μmol h^{-1} of N_2 fixed products formation rate).[16,17] The high voltage derived from TENG can be used to excite gases, such as N_2 and O_2, to generate triboelectric plasma.[18] High-energy electrons can interact with gas molecules to generate electronic excited states, vibrational excited states, and other active intermediates, which can improve the reaction kinetics and thermodynamically unfavorable chemical reactions under mild conditions.[19] Concurrently, triboelectric plasma can directly connect the TENG and the chemical reaction, reducing the energy loss caused by electrical energy management and storage.[20] The high substrate concentration and fast reaction speed in gas plasma effectively solve the problems of the low substrate concentration and hydrogen evolution in aqueous solutions.[21] Triboelectric plasma has the advantages of switching at any time, mild reaction conditions, and fast response speed, and exhibits potential compatibility with intermittent and irregular mechanical energy.[22] Therefore, mechanical-energy-driven triboelectric plasma is expected to become a small-scale N_2-fixation method with high efficiency and zero CO_2 emissions as no fossil fuels are required. Recently, some static and flow types of triboelectric plasma have been used for CO_2 reduction[19,23] or N_2 oxidation reaction,[24] but the activity and efficiency conversion of electrical to chemical energy are low. Because the average energy of electrons in the static or flow-type triboelectric plasma is large, it often causes the reaction to occur via a high-energy reaction pathway or serious heating effect.[25] Therefore, it is urgent to develop a novel type of triboelectric plasma for efficient N_2 fixation reaction.

This study reports an N_2 oxidation reaction using mechanical-energy-driven triboelectric plasma jet, which is at room temperature and atmospheric pressure, and using air directly as the raw material (Figure 1B). At the optimal distance of 2.0 mm, the NO_X formation rate was 4.82 μmol h^{-1}, which is 23-fold higher than the optimal activity of the current reported TENG-driven N_2 fixation reaction. The electrical to chemical energy conversion efficiency (η_{ele-NO_X}) was 4.92%. The electrical energy cost (EEC) for NO_X production was 1.76 MJ mol^{-1} N^{-1}, and the energy cost was the best record in the reported plasma N_2 fixation reactions at room temperature and atmospheric pressure. The reaction mechanism was investigated using optical emission spectroscopy (OES) and plasma simulation. Finally, a wind-driven N_2 fixation field investigation was conducted and a maximum NO_X yield of 8.09 μmol h^{-1} was obtained. This study provides an effective strategy for the efficient use of mechanical energy to drive the N_2 fixation reaction.

[1]Key Lab for Special Functional Materials, Ministry of Education, National & Local Joint Engineering Research Center for High-efficiency Display and Lighting Technology, School of Materials Science and Engineering, and Collaborative Innovation Center of Nano Functional Materials and Applications, Henan University, Kaifeng 475004, China

[2]Institute of Aero-engine, School of Mechanical Engineering, Xi'an Jiaotong University, Xi'an 710049, People's Republic of China

[3]Lead contact

*Correspondence:
zhangbao@henu.edu.cn (B.Z.),
chenggang@henu.edu.cn (G.C.),
zld@henu.edu.cn (Z.D.)

https://doi.org/10.1016/j.checat.2023.100647

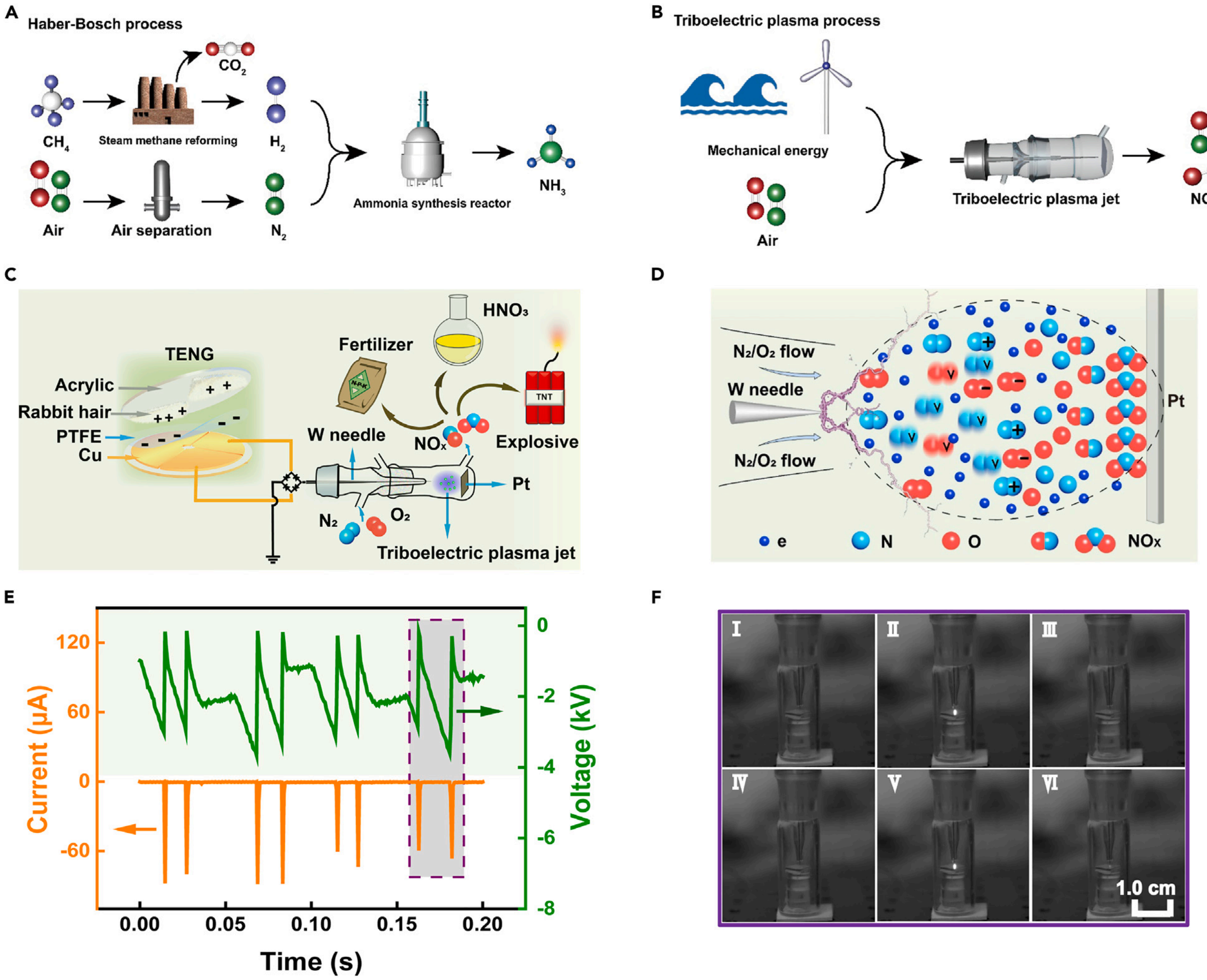

Figure 1. Mechanical-energy-induced N_2 oxidation system driven by a triboelectric plasma jet

(A) Industrial Haber-Bosch process.

(B) Triboelectric plasma-jet-driven N_2 fixation.

(C) Schematic diagram of the experimental device.

(D) Diagram of N_2 oxidation using a triboelectric plasma jet.

(E) Current and voltage curves of the triboelectric plasma jet versus time.

(F) High-speed photographs of the triboelectric plasma jet evolution. Reaction conditions: TENG rotational speed, 300 rpm; discharge distance, 2.0 mm; V_{N_2}/V_{O_2} ratio, 80:20; gas flow rate, 2.0 L min^{-1}; negative polarity; room temperature (25°C); and atmospheric pressure.

RESULTS AND DISCUSSION

N_2 oxidation reaction using the mechanical-energy-driven triboelectric plasma jet

Figure 1C shows the N_2 oxidation system using the mechanical-energy-driven triboelectric plasma jet. The reaction system consists of three parts, namely the TENG, rectifier bridge, and triboelectric plasma jet N_2 oxidation reactor. The TENG can collect natural mechanical energy (wind, water wave, raindrop, and other forms of energy) and convert it into electrical energy to provide a driving force for the triboelectric plasma jet.[26,27] The triboelectric plasma jet N_2 oxidation reactor consists of a nozzle and a needle-plate gas discharge device. When rabbit hair contacts with the polytetrafluoroethylene (PTFE) film on the copper electrode, positive and negative triboelectric charges are generated on the surface of the rabbit hair and PTFE film, respectively, and induced charges are generated on the surface of the copper

Please cite this article in press as: Wang et al., Efficient N_2 fixation in air enabled by mechanical-energy-driven triboelectric plasma jet, Chem Catalysis (2023), https://doi.org/10.1016/j.checat.2023.100647

electrode. Charge transfer occurs between the copper electrodes when the rabbit hair position changes, and electrical signals are generated. When the TENG output voltage exceeds the threshold voltage of the N_2/O_2 gas mixture (V_{N_2}: V_{O_2} = 80:20), the mixed gas ejected from the nozzle between the needle-plate electrodes is ionized, producing triboelectric plasma (see Figures S1 and 1D). According to the literature, in half a cycle, the output voltage of TENG increases linearly with the increase of the TENG rotational speed.[22] When the output voltage of TENG reaches the threshold voltage of N_2/O_2 mixture gas, gas discharge occurs, and the external circuit is connected. Then, a pulsed current is generated and the voltage difference is decreased to zero. When the output voltage of TENG is not enough to produce N_2/O_2 mixed gas discharge, the discharge pulsed current is not produced, and the output voltage is linearly increased with the output voltage of the TENG. Triboelectric plasma contains numerous electrons that can interact with N_2 and O_2 molecules to promote the oxidation of N_2, achieving NO_X products. Figure 1E shows the electrical curve of the triboelectric plasma jet at room temperature and normal pressure when the TENG rotational speed was 300 rpm, discharge distance (*d*) was 2.0 mm, flow rate of N_2/O_2 mixed gas (V_{N_2}: V_{O_2} = 80:20) was 2.0 L min^{-1}, and at negative polarity. In half a cycle, two discharge voltage peaks (*V*) of approximately 2.8–3.6 kV were generated, accompanied by a discharge current pulse peak (*I*) of approximately 59–87 μA (gray box in Figure 1E). These electrical signals correspond to the generation of the triboelectric plasma jet. Figure 1F shows a high-speed camera photographic image of the evolution process of the triboelectric plasma jet. The triboelectric plasma jet formation process can be divided into three stages, namely the before, during, and after breakdown stages. The duration of a single pulse was approximately 2.0 ms, and the length of the triboelectric plasma jet was 2.0 mm (Figure S2).

Effects of the TENG rotational speed, mixed gas flow rate, and N_2/O_2 volume ratio on the N_2 oxidation reaction

Next, the influence of the TENG rotational speed on the N_2 oxidation reaction was investigated. The frequency of the generated triboelectric plasma increased with an increasing TENG rotational speed; however, the number of discharges and *V* and *I* in each cycle remained unchanged (Figure 2A). The results show that the state of the triboelectric plasma formed at different rotational speeds was approximately the same. When the rotational speed was increased from 240 to 360 rpm, the average power (P_{ave}) of the triboelectric plasma increased from 1.50 to 2.90 mW, the NO_X generation rate (r_{NO_X}) increased from 3.96 to 5.95 μmol h^{-1}, the η_{ele-NO_X} was 4.60–5.93%, and the EEC for NO_X production was 1.46–1.88 MJ mol^{-1} N^{-1} (Figures 2B–2C). These results show that the mechanical-energy-driven triboelectric plasma jet N_2 oxidation system exhibited good compatibility and adaptability to natural mechanical energy fluctuations in the environment. The influence of the N_2/O_2 mixed gas flow rate on the N_2 oxidation performance was then studied. When the N_2/O_2 flow was increased from 0.5 to 3.0 L min^{-1}, *V*, *I*, and P_{ave} remained unchanged, and r_{NO_X} and η_{ele-NO_X} first increased and then decreased. When the N_2/O_2 mixed gas flow rate was 2.0 L min^{-1}, the maximum r_{NO_X} and η_{ele-NO_X} values were 4.82 μmol h^{-1} and 4.92%, respectively. The minimum EEC value for NO_X production was 1.76 MJ mol^{-1} N^{-1} (Figures S3 and S4). Hence, the η_{ele-NO_X} and EEC values for NO_X production remained at a high and low level, respectively, with the change in the N_2/O_2 mixed gas flow rate. These results show that our system has good compatibility with the N_2/O_2 mixed gas flow rate.

The influence of the N_2/O_2 volume ratio in the mixed gas on the N_2 oxidation performance was then studied (Figures S5 and S6). The discharge voltage and discharge

Please cite this article in press as: Wang et al., Efficient N_2 fixation in air enabled by mechanical-energy-driven triboelectric plasma jet, Chem Catalysis (2023), https://doi.org/10.1016/j.checat.2023.100647

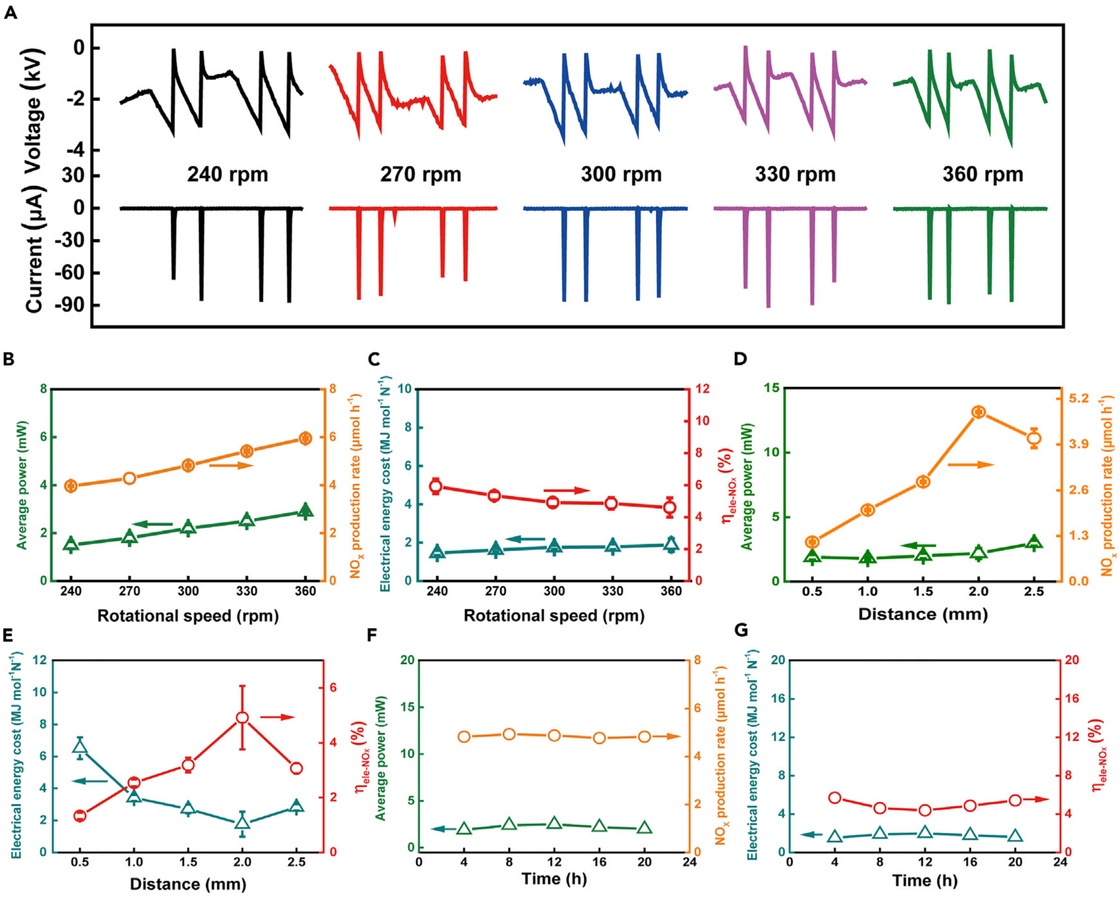

Figure 2. Influence of parameters on the N_2 oxidation reaction

(A) Voltage and current curves versus the TENG rotational speed.

(B) Average power and NO_X production rate versus the TENG rotational speed.

(C) Electrical energy cost (EEC) for NO_X production and η_{ele-NO_X} versus the TENG rotational speed. Reaction conditions: discharge distance, 2.0 mm; V_{N_2}/V_{O_2} ratio, 80:20; gas flow rate, 2.0 L min^{-1}; negative polarity; room temperature (25°C); and atmospheric pressure.

(D) Average power and NO_X production rate versus the discharge distance.

(E) EEC for NO_X production and η_{ele-NO_X} versus the discharge distance.

(F) Average power and NO_X production rate at a discharge distance of 2.0 mm and reaction time of 20 h.

(G) EEC for NO_X production and η_{ele-NO_X} at a discharge distance of 2.0 mm and reaction time of 20 h. Reaction conditions: TENG rotational speed, 300 rpm; V_{N_2}/V_{O_2} ratio, 80:20; gas flow rate, 2.0 L min^{-1}; negative polarity; room temperature (25°C); and atmospheric pressure.

current curves changed significantly with an increase in the N_2/O_2 volume ratio, mainly because the discharge voltage of the mixed gas with different N_2/O_2 volume ratios differed. The calculated P_{ave} did not differ considerably. When the V_{N_2}:V_{O_2} ratio was 80:20, r_{NO_X} and η_{ele-NO_X} were at their highest value, and the EEC value for NO_X production was at its lowest. This result shows that our system can directly use air for N_2 fixation without separating N_2 from the air, effectively reducing the energy consumption and carbon emissions of the entire system.

According to the literature,[19,23,24] including triboelectric plasma reported in our article, the models of triboelectric plasma are mainly divided into three types: static,[23,24] flow,[19] and nozzle. The static type of triboelectric plasma has been used for CO_2 reduction[23] and N_2 fixation reaction,[24] where the gas was not flowing but static. Recently, the flow type of triboelectric plasma has been used for CO_2 reduction,[19] where the gas was not static but flowing at the flow rate of 0.2–12.5 mL min^{-1}. Different from the static and flow types of triboelectric plasma in

Please cite this article in press as: Wang et al., Efficient N_2 fixation in air enabled by mechanical-energy-driven triboelectric plasma jet, Chem Catalysis (2023), https://doi.org/10.1016/j.checat.2023.100647

the literature, we first increased the gas flow rate to 2 L min^{-1}, which is much higher than that in the flow type of triboelectric plasma (0.2–12.5 mL min^{-1}) and then introduced a nozzle to change the plasma dynamics. The influence of the reactor types (static, flow, and nozzle type) of the triboelectric plasma on the N_2 reaction activity was then investigated. The discharge current and discharge voltage of the three types of reactors exhibited little change, and the P_{ave} of the three types of reactors were similar; however, r_{NO_X} and η_{ele-NO_X} increased and EEC for NO_X production gradually decreased. The above results show that the gas flow and nozzle play an important role in improving the activity and efficiency of the N_2 oxidation reaction. The gas flow and nozzle can effectively reduce the mixed gas residence time in the plasma area, vibrational-translational relaxation losses, and the reverse reaction of the Zeldovich mechanism,[2,28] thus improving the reaction activity and energy efficiency and reducing the energy consumption (Figures S7 and S8).

Effect of needle-plate distance

The influence of needle-plate distance (d) was then investigated. When d was increased from 0.5 to 2.5 mm, the number of discharge pulses in a half cycle decreased from 2 to 1, V increased from 3.1 to 5.0 kV, and I increased from 63.9 to 96.5 μA (Figure S9). An increasing d hinders the formation of the discharge between the needle and plate electrode, which requires a higher voltage to realize the gas discharge, resulting in a reduction in the number of discharges in each cycle. Therefore, the amount of charge per discharge pulse increases, resulting in a higher discharge current. As shown in Figures 2D and 2E, as d increased from 0.5 to 2.0 mm, P_{ave} increased from 1.90 to 2.20 mW, r_{NO_X} increased from 1.13 to 4.82 μmol h^{-1}, η_{ele-NO_X} increased from 1.33% to 4.92%, and EEC for NO_X production decreased from 6.51 to 1.76 MJ mol^{-1} N^{-1}. When d was further increased to 2.5 mm, η_{ele-NO_X} decreased significantly to 3.06% and EEC for NO_X production increased to 2.82 MJ mol^{-1} N^{-1}. η_{ele-NO_X} and EEC for NO_X production achieved their optimal values of 4.92% and 1.76 MJ mol^{-1} N^{-1}, respectively, at d = 2.0 mm.

To validate the measured NO_X products that derived from N_2 oxidation reaction, we operated the control experiment in the absence of triboelectric plasma (Figure S10A). Compared with the presence of triboelectric plasma, without triboelectric plasma, no NO_X was observed, indicating the necessity of triboelectric plasma in yielding NO_X. To further confirm that the generated NO_X products in the N_2 oxidation reaction originates from N_2 and O_2 gas, we conducted an additional control experiment under different atmospheric conditions with triboelectric plasma. Under the triboelectric plasma, null NO_X products was generated under Ar, O_2, or N_2 conditions, excluding the false-positive contribution of the synthetic precursors and other possible triboelectric plasma reactions.

To further investigate whether the NO_X originated from N_2 fixation reaction, the isotope labeling experiments were designed using $^{15}N_2$ as the feeding gas (Figures S10B and S10C). Due to the low concentration of NO_X in the N_2 oxidation, the isotope labeling experiments were carried out for 2 days, using $^{15}N_2$ as the N source, in a sealed glass reactor. The generated NO_X products were analyzed by Nu isotope mass spectrometry. For the comparison, using the $^{14}N_2$ and $^{16}O_2$ as the mixed gas, there is a striking peak at m/z = 30 in the mass spectrum, which was attributed to the $^{14}N^{16}O$. Using the $^{15}N_2$ and $^{16}O_2$ as the mixed gas, there is a peak at m/z = 31 in mass spectrum, which was assigned to the $^{15}N^{16}O$, indicating that the N atom of the NO_X products stems from N_2 feedstock. Collectively, the above results imply that the NO_X product in the triboelectric plasma N_2 oxidation reaction is indeed from the N_2 feedstocks.

Please cite this article in press as: Wang et al., Efficient N_2 fixation in air enabled by mechanical-energy-driven triboelectric plasma jet, Chem Catalysis (2023), https://doi.org/10.1016/j.checat.2023.100647

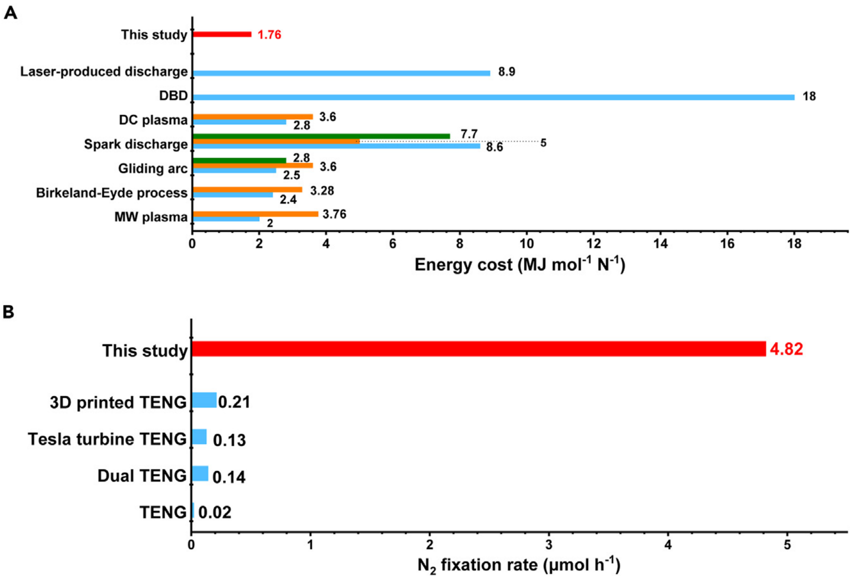

Figure 3. Comparison of different types of plasma and different mechanical energy sources

(A) Energy cost of different types of plasma used for N_2 oxidation at room temperature and atmospheric pressure.

(B) N_2 fixation rate using different types of mechanical energy sources for N_2 oxidation.

To test the stability of the system under the reaction conditions of TENG rotational speed of 300 rpm, d of 2.0 mm, and N_2/O_2 mixed gas flow rate of 2.0 L min^{-1}, the N_2 oxidation reaction was continuously performed under negative polarity and normal temperature and pressure for 20 h (Figures 2F and 2G). The resulting P_{ave}, r_{NO_X}, η_{ele-NO_X}, and EEC values for NO_X production were 1.90–2.50 mW, 4.77–4.93 μmol h^{-1}, 4.38%–5.69%, and 1.52–1.98 MJ mol^{-1} N^{-1}, respectively. These results show that the system exhibited good long-term stability.

The triboelectric plasma jet is a mechanical-energy-driven non-thermal plasma. Different types of plasma, such as dielectric barrier discharge[29] and microwave plasma,[2] were compared to illustrate the advantages of the triboelectric plasma jet for N_2 fixation (Figure 3A; Table S1).[7,29–38] To the best of our knowledge, our system, compared with the reported plasma N_2 fixation reactions at room temperature and atmospheric pressure, exhibited the lowest energy consumption for NO_X production of 1.76 MJ mol^{-1} N^{-1} (calculated based on the total output energy provided for triboelectric plasma; see Note S1 and Figure S11). Although some literature has reported that the energy cost of atmospheric spark plasma[25] or soft-jet-pulsed plasma[39] is particularly low, reaching 0.4 MJ mol^{-1} (atmospheric spark plasma) or 0.42 MJ mol^{-1} (pulsed plasma) respectively, the calculation method of energy cost in the literature is different from that calculated in this study. The lower energy cost calculated in the previous literature was based on the estimated power absorbed in the plasma, not considering the energy that was used for maintaining the plasma.[25,39] According to the literature, the power adsorbed in the plasma only accounts for 2%–5% of the electrical energy provided by the power supply.[25,39] If the energy used for maintaining the plasma was considered based on this paper, the energy cost of the atmospheric spark plasma and pulsed plasma reaches 8 and 8.4 MJ mol^{-1}, respectively, which are far higher than that reported in this paper.[25,39]

Please cite this article in press as: Wang et al., Efficient N_2 fixation in air enabled by mechanical-energy-driven triboelectric plasma jet, Chem Catalysis (2023), https://doi.org/10.1016/j.checat.2023.100647

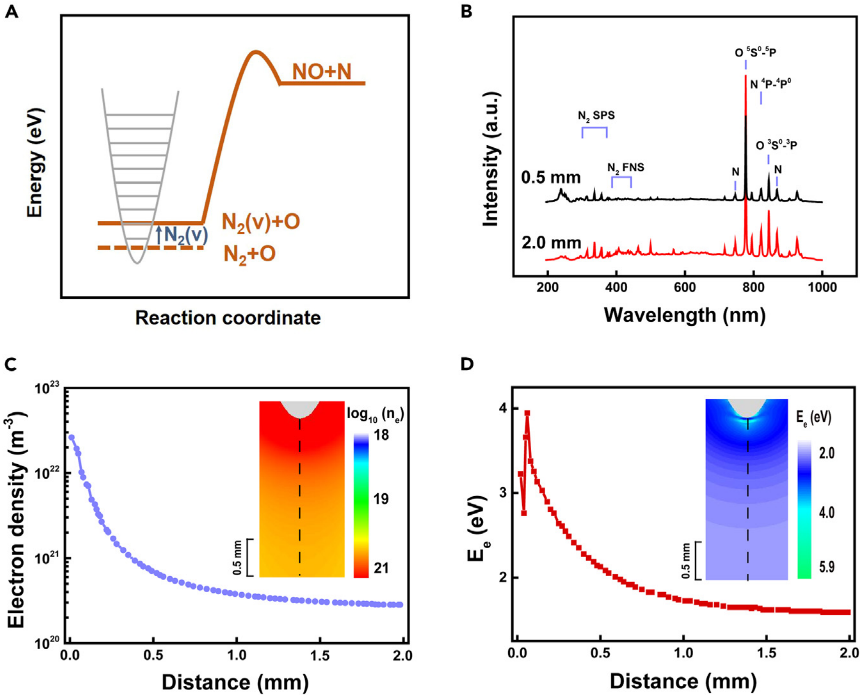

Figure 4. Proposed mechanism for triboelectric plasma N_2 oxidation

(A) Potential energy surfaces of the N_2 activation processes in the triboelectric plasma.

(B) OES at 0.5 and 2.0 mm.

(C) Electron density versus the distance from the tip at the central axis at 70 ns.

(D) Average electron energy versus the distance from the tip at the central axis at 70 ns.

Furthermore, the activity of the N_2 fixation reaction driven by a TENG directly using mechanical energy was compared with those reported in the literature,[15–17] as shown in Figure 3B and Table S2. The reported activity of TENG-driven N_2 fixation is extremely low, with a general order of magnitude of 0.1 μmol h^{-1} of N_2 fixed product formation rate (obtained at TENG speeds of 2,000–5,000 rpm).[15–17] The fixed NO_X yield obtained from our system was 4.82 μmol h^{-1} (obtained at the TENG speed of 300 rpm), which is approximately one order of magnitude higher than the previously reported activities.[15–17]

N_2 oxidation reaction mechanism

The reaction mechanism of the triboelectric plasma jet oxidation of N_2 was investigated to explore the reason for the high reactivity and energy efficiency of the triboelectric plasma jet. The reported N_2 oxidation reaction mainly occurs through two pathways, namely through the electron collision dissociation (ECD) and vibrational excitation dissociation (VED) pathways (Figure 4A).[40] The energy barrier of the ECD pathway is 9.75 eV.[28] The reaction process is defined as follows:

$$N_2 + e^- \rightarrow N + N + e^- \ \Delta H_1 = 9.75 \text{ eV} \qquad \text{(Equation 1)}$$

$$O_2 \rightarrow O + O \ \Delta H_2 = 5.2 \text{ eV} \qquad \text{(Equation 2)}$$

$$N + O \rightarrow NO \ \Delta H_3 = -6.3 \text{ eV} \qquad \text{(Equation 3)}$$

The energy barrier of the whole VED process is 3.0 eV.[2] This mechanism is also called the non-thermal Zeldovich mechanism (Figure 4A).[2] In the reaction process, N_2

Please cite this article in press as: Wang et al., Efficient N_2 fixation in air enabled by mechanical-energy-driven triboelectric plasma jet, Chem Catalysis (2023), https://doi.org/10.1016/j.checat.2023.100647

molecules are excited step by step from the lowest vibrational level to a higher vibrational level $N_2(v)$ until the energy barrier of the VED process is overcome. The energy barrier of each step in the VED process is 0.3 eV, which is the most efficient N_2 dissociation process for non-thermal plasma.[28,41–43]

$$O + N_2(v) + e^- \rightarrow NO + N + e^- \ \Delta H_4 = 3\ eV \qquad \text{(Equation 4)}$$

$$N + O_2 \rightarrow NO + O\ \Delta H_5 = -1\ eV \qquad \text{(Equation 5)}$$

OES is an effective method to study the active species in the triboelectric plasma N_2 oxidation reaction. High-performance OES (QEpro) was used to measure the emission spectra in the reaction process at the points where *d* was 0.5 and 2.0 mm, as shown in Figure 4B. In the two spectrograms, two groups of relatively wide spectral bands appeared at 311–380 and 390–470 nm, corresponding to the second positive band system of the N_2 molecule, which was attributed to the transition of the N_2 molecule from the $C^3\Pi_g$ to $B^3\Pi_g$ state,[44] and the first negative band system of N_2, which was attributed to the transition of the N_2 molecule from the $B^2\Sigma_u^+$ to $X^2\Sigma_u^+$ state, respectively.[44] These two bands correspond to the transition of the N_2 vibrational energy level, forming active N_2 molecules, which directly demonstrates the existence of the VED process. Two strong emission peaks were observed at 777.5 and 844.7 nm, which correspond to the $^5S^0$ to ^5P and $^3S^0$ to ^3P transitions of O atoms,[44] respectively, indicating that a large number of O atoms were generated during N_2 oxidation.[44] Three emission spectra peaks of the N atom were generated at 742, 822, and 868 nm, which represent the excited N atoms generated during N_2 oxidation.[44] The intensity of the emission spectrum peaks of the N_2 molecule and O and N atoms at 2.0 mm, compared with 0.5 mm, significantly increased, indicating that *d* = 2.0 mm is more conducive to the occurrence of the N_2 VED process.

The space and energy distribution of electrons in triboelectric plasma are crucial when exploring the N_2 oxidation reaction mechanism; therefore, the electron density (n_e) and average electron energy (E_e) distribution were calculated, and the triboelectric plasma evolution process was simulated in different spatial positions, as shown in Figure S12. When *d* increased from 0.5 to 2.5 mm, a cylindrical plasma channel was formed in the needle-plate gap, where n_e and E_e were higher at the central axis of the channel and lower at the edge of the channel. At *d* = 2.0 mm, the n_e and E_e distribution in the triboelectric plasma were the most uniform at 7.86×10^{19} m^{-3} and 0.36 eV, respectively (the height of the cylindrical area was 2.0 mm and the diameter were 1.0 mm). E_e gradually decreased and the total number of electrons in the plasma channel increased with an increasing *d*. For example, when *d* was increased from 0.5 to 2.0 mm, the n_e in the plasma channel increased from 6.69×10^{19} m^{-3} to 7.86×10^{19} m^{-3}, and the E_e of the plasma in the channel decreased from 0.95 to 0.36 eV. Figure S13 shows the evolution of the triboelectric plasma n_e and E_e with time at *d* = 2.0 mm. The shape of the triboelectric plasma changed from ellipsoid to cylindrical with increasing time, and n_e increased from 5.02×10^{17} m^{-3} to 7.86×10^{19} m^{-3}, whereas E_e decreased from 0.41 to 0.36 eV.

Figures 4C and 4D shows the changes in n_e and E_e at the central axis of the plasma channel and the distance from the needle tip when *t* = 70 ns and *d* = 2 mm. The n_e and E_e at the tip of the tungsten needle were 2.1×10^{22} m^{-3} and 3.5 eV, respectively, and changed to 2.8×10^{20} m^{-3} and 1.6 eV, respectively, at the plate electrode. The electron energy distribution function (EEDF) at five representative points (0.4, 0.8, 1.2, 1.6, and 2.0 mm from the tip) were calculated and are shown in Figure S14. The average energy of almost all electrons from point i to point v was <9.8 eV; therefore, the ECD process has difficulty occurring due to the high energy

Please cite this article in press as: Wang et al., Efficient N_2 fixation in air enabled by mechanical-energy-driven triboelectric plasma jet, Chem Catalysis (2023), https://doi.org/10.1016/j.checat.2023.100647

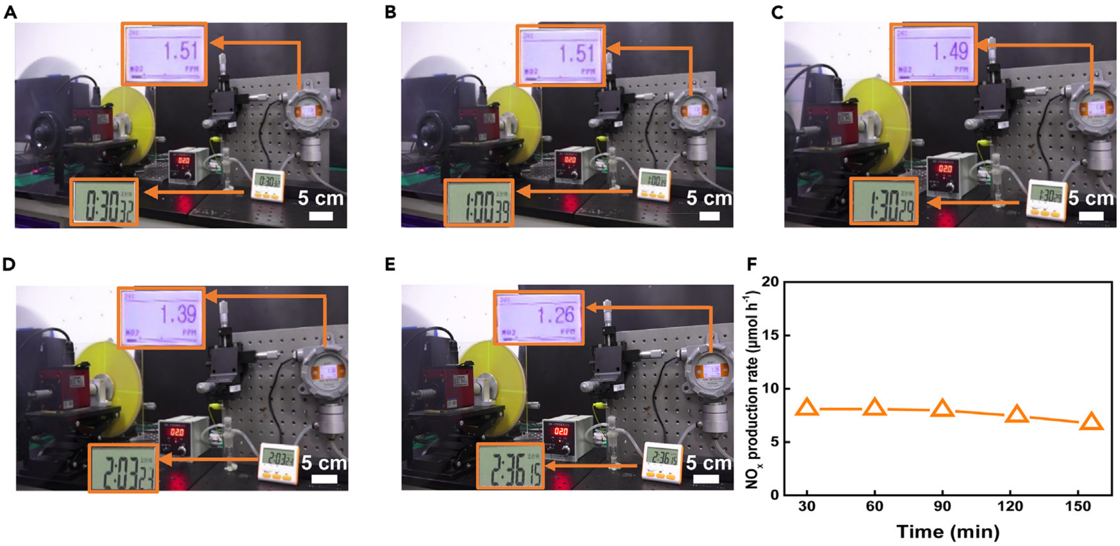

Figure 5. Field test of the wind-energy-driven triboelectric plasma jet for N_2 oxidation
(A–E) NO_X detector indicator at (A) 30, (B) 60, (C) 90, (D) 123, and (E) 156 mins.
(F) NO_X production rate versus time.

barrier. Approximately 88.0% of the electrons from point i to point v had an average energy <3.0 eV. These low-energy electrons can be excited step by step through the ''ladder'' method to finally overcome the energy barrier for the VED process to occur. Therefore, the ECD process cannot occur in the plasma channel, and the VED process occurs in the entire channel. Compared with the average energy of electrons in traditional plasma (for example, the average energy of electrons in microwave plasma is 1.2 eV[2]), the average energy of the electrons in the mechanical-energy-driven triboelectric plasma jet was lower, which is conducive to the VED process with low energy barriers and inhibits the ECD process with high energy barriers. Therefore, the triboelectric plasma jet exhibits high activity and low energy consumption.

Field test

The previous sections indicated that fluidic triboelectric plasma jet can induce an efficient N_2 fixation reaction and that the reaction system can also collect natural mechanical energy. To confirm whether the triboelectric plasma jet N_2 oxidation system can effectively use natural mechanical energy, a wind-energy-driven field experiment was performed. Figures 5A–5E show that, at wind speeds of 1.8–2.2 m s^{-1}, the concentration of NO_X was 1.51, 1.51, 1.49, 1.39, and 1.26 ppm at 30, 60, 90, 123, and 156 min, respectively. The corresponding NO_X generation rates were 8.09, 8.09, 7.98, 7.45, and 6.75 μmol h^{-1} (Figure 5F), respectively. The above results show that the system could directly use natural wind energy to efficiently fix N_2.

To further illustrate the advantages of our system, the thermal catalytic and photocatalytic N_2 fixation processes were compared. The traditional thermal catalytic N_2 fixation reaction requires a large amount of fossil fuel as well as hydrogen and metal catalysts, and the reaction conditions are harsh.[45] Additionally, a large amount of CO_2 is emitted, which causes the greenhouse effect.[6] Compared with traditional thermal catalysis, our system does not require fossil energy or hydrogen and metal catalysts. The CO_2 emission is almost 0 and the reaction conditions are mild. Additionally, air can be directly used as a raw material without N_2 separation, further

Please cite this article in press as: Wang et al., Efficient N_2 fixation in air enabled by mechanical-energy-driven triboelectric plasma jet, Chem Catalysis (2023), https://doi.org/10.1016/j.checat.2023.100647

reducing energy consumption. The energy cost of our system is 1.76 MJ mol^{-1} N^{-1}, which is also much higher than that of the industrial world-scale H-B process. After more than 100 years of improvement, the current energy cost of the H-B process has been close to the theoretical value of energy cost (about 0.5 MJ mol^{-1} N^{-1}). However, there is still much room for improvement in the energy cost of triboelectric plasma N_2 fixation reaction, because the current energy cost is far from the theoretical value of the Zeldovich mechanism (about 0.2 MJ mol^{-1} N^{-1}).[2] In the future, we can consider introducing catalysts or changing the structure of the reactor to further reduce the energy cost of the reaction. At present, the triboelectric plasma system driven by TENG is difficult to carry out in large-scale practical applications because of its low NOx content. In the future, series or parallel connection of the system can be considered to increase the activity of the whole system. The N_2 fixation reaction using light energy as an energy source was developed recently and is a promising way to fix N_2 under mild reaction conditions.[46] However, the narrow absorption range of the photocatalysts, low carrier separation efficiency, side reactions, and hydrogen evolution competitive reaction seriously inhibit the activity and energy efficiency of the N_2 reduction reaction.[47] The absolute activity of the photocatalytic N_2 fixation reaction at present is only 0.01–0.1 μmol h^{-1} of the N_2 fixed-products rate.[48,49] The system proposed in this study does not require catalysts, and only uses air as a raw material. The proposed system is simple, avoiding energy loss caused by complex processes, and has high activity and energy efficiency.

Conclusions

A mechanical-energy-driven triboelectric plasma jet was constructed in this study to achieve N_2 fixation at normal temperature and atmospheric pressure. The system exhibited good compatibility with natural mechanical energy and gas flow rate fluctuations. At a discharge distance of 2.0 mm, the NO_X production rate was 4.82 μmol h^{-1}, which is an activity value 23-fold higher than those of the previously reported N_2-fixation systems driven by TENGs directly using mechanical energy at normal temperature and pressure. The electrical to chemical energy conversion efficiency was 4.92% and EEC for NO_X production was 1.76 MJ mol^{-1} N^{-1}. The EEC achieved in this study was lower than those of the previously reported plasma N_2 fixation reactions at room temperature and atmospheric pressure. The emission spectra and plasma simulation results show that the reason for the high activity and efficiency of the mechanical-energy-driven triboelectric plasma jet is that the average energy of the electrons in the plasma is low, which is conducive to the VED process with low energy barriers. Finally, the proposed system could efficiently use natural wind energy, and the maximum NO_X generation rate was 8.09 μmol h^{-1}. In the future, the mechanical energy collection device can be further optimized and improved to increase the energy conversion efficiency of the entire system.

EXPERIMENTAL PROCEDURES

Resource availability

Lead contact

Further information and requests for resources and materials should be directed to and will be fulfilled by the lead contact, Gang Cheng (chenggang@henu.edu.cn).

Materials availability

This study did not generate new unique materials.

Data and code availability

Data from this study are available from the lead contact upon reasonable request.

Fabrication of the free-standing TENG

The free-standing TENG was selected in this study to generate triboelectric plasma jet. The free-standing TENG consisted of three parts, namely the electrode, independent layer, and triboelectric layer. A 60.0-μm-thick copper film was coupled to a 0.3-cm-thick printed circuit board (Φ = 25.0 cm) as the electrode layer, which was adhered to a 25-cm-diameter, 0.4-cm-thick polymethylmethacrylate (PMMA) substrate to form the stator. The copper electrode was divided into four sectors of the same size. Each sector accounted for one-quarter of the PMMA area. The interval between the copper electrodes in adjacent sectors was 1.0 cm. The copper electrodes in two sectors were connected by copper wires. PTFE with a thickness of 0.06 mm was used as an independent layer, which was respectively pasted on the four copper electrode surfaces. Rabbit hair was used as the triboelectric layer, and was divided into two fan-shaped areas of equal size, which were the same size as the fan-shaped copper electrode. The rabbit hair in the two fan-shaped areas was alternately pasted on the round 25-cm-diameter and 0.6-cm-thick PMMA substrate to form the rotor. The rotor was connected to the motor shaft through a flange mounting shaft; the stator was vertically fixed above the rotor. The free-standing TENG was connected to the rectifier bridge to provide unidirectional pulse current and voltage.

Mechanical-energy-driven triboelectric plasma jet N_2 oxidation reaction

The triboelectric plasma jet N_2 oxidation reaction device consisted of three parts, namely a nozzle-shaped glass reactor (outer and inner diameters of 2.6 and 1.8 cm, respectively), and two gas discharge electrodes (tungsten needle with a 5-μm curvature radius, and a 1.0 × 1.0-cm platinum sheet). The tungsten needle was in the nozzle of the glass reactor and connected with the negative polarity of the rectifier bridge, and the platinum plate was fixed at the bottom of the glass reactor and connected with the positive polarity of the rectifier bridge; the two were placed vertically. N_2/O_2 mixed gas was connected to the glass reactor through a gas inlet using a hose with an inner diameter of 0.3 cm. The product NO_X and unreacted N_2 and O_2 were connected to a NO_X gas detector through the gas outlet (Shenzhen Xinyangwei Technology Development). In this study, the NO_X product concentration displayed on the NO_X gas detector was uniformly represented by the value of NO_2 concentration (ppm). The gas flow rate was controlled using a mass flowmeter (Beijing Seven Star Company). A conical nozzle (outer and inner diameter of 3.0 and 1.5 mm, respectively) was attached at the gas inlet of the glass reactor to spray gas in the form of a jet. The N_2 oxidation reaction of mechanical-energy-driven triboelectric plasma jet was performed under the following TENG conditions: rotational speed of 300 rpm, negative polarity, discharge distance of 2.0 mm, and an N_2/O_2 mixture ($V_{N_2}:V_{O_2}$ = 80:20) flow rate of 2.0 L min^{-1}. The effects of the TENG rotational speed, discharge distance (d), mixed gas flow rate, N_2/O_2 volume ratio, reactor type on the activity, EEC for NO_X production, and energy efficiency were investigated. Photographic images of the triboelectric plasma jet were captured using a high-speed camera (TMX7510, Phantom, York Technologies) at a rate of 1,000 images per second. The emission spectrum of the triboelectric plasma jet was detected using a monochromator adjustable light source (Beijing Newbit Technology).

For the isotope labeling experiment, the substrate was $^{15}N_2$ (99% atom of ^{15}N, Wuhan Newradar Special Gas)/$^{16}O_2$ mixed gas, and the N_2 oxidation reaction was operated in a sealed glass reactor for 2 days. The NO_X products were analyzed by Nu isotope mass spectrometry.

Please cite this article in press as: Wang et al., Efficient N_2 fixation in air enabled by mechanical-energy-driven triboelectric plasma jet, Chem Catalysis (2023), https://doi.org/10.1016/j.checat.2023.100647

EEC and η_{ele-NO_X}

The triboelectric plasma electrical signals were simultaneously obtained using two electrometers (Keithley 6514) at different ranges. One electrometer was used to test the discharge current (I) and the other was used to test the discharge voltage (V). The inherent capacitance (C) of a free-standing TENG is constant,[50] and the voltage of TENG is proportional to the amount of transferred charge (Q), defined as:

$$C = \frac{Q}{V} \qquad \text{(Equation 6)}$$

where Q is the amount of transferred charge. In half a cycle, the maximum output energy (E_{max}) of the TENG can be determined as:

$$E_{max} = \frac{1}{2}Q_{max} \cdot V_{oc} = \frac{1}{2}C \cdot {V_{oc}}^2 \qquad \text{(Equation 7)}$$

where, Q_{max} is the maximum transferred charge of the TENG, and V_{OC} is the open circuit voltage of the TENG. For each triboelectric plasma discharge peak, the output electric energy (E) can be determined as:

$$E = \frac{1}{2}Q_1 \cdot V_1 = \frac{1}{2}C \cdot {V_1}^2 \qquad \text{(Equation 8)}$$

where Q_1 is the amount of charge transferred during discharging process, and V_1 is the peak voltage of the plasma discharge process. Therefore, E can also be expressed as:

$$E = E_{max} \cdot \left(\frac{V_1}{V_{oc}}\right)^2 \qquad \text{(Equation 9)}$$

The average power (P_{ave}) of the triboelectric plasma can be calculated as:

$$P_{ave} = \frac{\sum_1^n E_n}{t} \qquad \text{(Equation 10)}$$

where E_n is the electric energy of the n^{st} triboelectric plasma peaks during the total discharge process, and t is the time of the total discharge process. The NO_X production rate (r_{NO_X}) can be calculated as:

$$r_{NO_X} = C_{NO_X} \cdot Q_{N_2/O_2} \cdot 60 \qquad \text{(Equation 11)}$$

where C_{NO_X} is the concentration of NO_X (μmol L^{-1}) and Q_{N_2/O_2} is the flow rate of the N_2/O_2 mixture (L min^{-1}). The EEC for NO_X production can be calculated using Equation 7:

$$\text{EEC} = \frac{P_{ave} \cdot 3600}{r_{NO_X}} \qquad \text{(Equation 12)}$$

The η_{ele-NO_X} can be calculated using Equation 8:

$$\eta_{ele-NO_X} = \frac{r_{NO_X} \cdot \Delta G_r}{P_{ave} \cdot 3600} \qquad \text{(Equation 13)}$$

where ΔG_r is the Gibbs free energy change of the N_2 oxidation reaction to NO (86.55 kJ mol^{-1}).

Wind-driven field test

In the field experiment, the electric motor was replaced with a fan, which can directly use natural wind energy. The other reaction units were essentially the same as those used in the TENG-driven N_2 oxidation system. The wind speed in the field test was 1.8–2.2 m s^{-1} for 3 h.

Please cite this article in press as: Wang et al., Efficient N_2 fixation in air enabled by mechanical-energy-driven triboelectric plasma jet, Chem Catalysis (2023), https://doi.org/10.1016/j.checat.2023.100647

Triboelectric plasma jet simulation

The triboelectric plasma jet was modeled following the fluid approach in the framework of the PASSKEy code.[51] The Poisson equations for electric field coupling with a set of continuity equations of electrons, electron energy, ions, and other chemical active species were solved:

$$\nabla(\varepsilon_0 \varepsilon_r \nabla \Phi) = -\rho \qquad \text{(Equation 14)}$$

$$E = -\nabla \Phi, \rho = \sum_{i=1}^{N_{ch}} q_i n_i \qquad \text{(Equation 15)}$$

$$\frac{\partial n_i}{\partial t} + \nabla \cdot \Gamma_i = S_i, i = 1, 2, 3....., N_{total} \qquad \text{(Equation 16)}$$

$$\Gamma_i = \left(\frac{q_i}{|q_i|}\right) \mu_i n_i E - D_i \nabla n_i, i = 1, 2, 3......N_{ch} \qquad \text{(Equation 17)}$$

where ε_0 and ε_r are the permittivity and relative permittivity, respectively; Φ is electric potential; E is the electric field; ρ_c is the dielectric surface charge; q_i and n_i are density and charge of specie i, respectively; N_{ch} is several the charged species; S_i represents the reaction and photoionization source terms; Γ_i is the flux solved based on the drift-diffusion approximation; μ_i is mobility; and D_i is the diffusion coefficient.

The equations were discretized over a 30 × 30-mm axisymmetric computational domain (see Figure S15). The red area represents the pin anode, the bottom line represents the cathode plane, and the blue area shows the region where continuity equations would be solved (in other regions, only Poisson's equation was solved). The mesh was refined to the size of 5 μm within the plasma domain and was further refined to 2 μm near the plane electrode. In the rest of the computational domain, the mesh size grew exponentially until the boundaries of the computational domain was reached.

The aim of the simulation was to obtain the spatial-temporal distribution of the electron, mean electron energy, and electric field, and thus a simplified reaction scheme was used, taking into account 17 species (N_2, O_2, e^-, N, N_2^+, N_3^+, $N_2(A^3\Sigma_u)$, $N_2(B^3\Pi_g)$, $N_2(C^3\Pi_u)$, O, $O(^1D)$, O^-, O_2^-, O_2^+, O_4^+ etc.) and 41 chemical reactions, as has been described in the literature.[52] The scheme was satisfactory in describing the evolution of the charged species and the phenomenon of gas heating in the studied period.

SUPPLEMENTAL INFORMATION

Supplemental information can be found online at https://doi.org/10.1016/j.checat.2023.100647.

ACKNOWLEDGMENTS

This study was funded by the National Natural Science Foundation of China (grant numbers 21902043 and 61974040).

AUTHOR CONTRIBUTIONS

Conceptualization, B.Z. and C.G.; methodology, B.Z., J.W., Y.L., and Z.H.Z.; software, Y.F.Z.; investigation, J.W., Q.L.R., H.J.C., and S.M.L.; writing – original draft, B.Z., J.W., and C.G.; writing – review & editing, B.Z. and C.G.; funding acquisition, B.Z. and C.G.; resources, B.Z. G.C., and Z.L.D; supervision, B.Z., G.C., and Z.L.D.

Please cite this article in press as: Wang et al., Efficient N_2 fixation in air enabled by mechanical-energy-driven triboelectric plasma jet, Chem Catalysis (2023), https://doi.org/10.1016/j.checat.2023.100647

DECLARATION OF INTERESTS

The authors declare no competing interests.

Received: January 4, 2023
Revised: February 23, 2023
Accepted: May 9, 2023
Published: May 31, 2023

REFERENCES

1. Han, G.F., Li, F., Chen, Z.W., Coppex, C., Kim, S.J., Noh, H.J., Fu, Z., Lu, Y., Singh, C.V., Siahrostami, S., et al. (2021). Mechanochemistry for ammonia synthesis under mild conditions. Nat. Nanotechnol. *16*, 325–330. https://doi.org/10.1038/s41565-020-00809-9.
2. Kelly, S., and Bogaerts, A. (2021). Nitrogen fixation in an electrode-free microwave plasma. Joule *5*, 3006–3030. https://doi.org/10.1016/j.joule.2021.09.009.
3. Suryanto, B.H.R., Matuszek, K., Choi, J., Hodgetts, R.Y., Du, H.L., Bakker, J.M., Kang, C.S.M., Cherepanov, P.V., Simonov, A.N., and MacFarlane, D.R. (2021). Nitrogen reduction to ammonia at high efficiency and rates based on a phosphonium proton shuttle. Science *372*, 1187–1191. https://doi.org/10.1126/science.abg2371.
4. MacFarlane, D.R., Cherepanov, P.V., Choi, J., Suryanto, B.H., Hodgetts, R.Y., Bakker, J.M., Ferrero Vallana, F.M., and Simonov, A.N. (2020). A roadmap to the ammonia economy. Joule *4*, 1186–1205. https://doi.org/10.1016/j.joule.2020.04.004.
5. Ashida, Y., Onozuka, Y., Arashiba, K., Konomi, A., Tanaka, H., Kuriyama, S., Yamazaki, Y., Yoshizawa, K., and Nishibayashi, Y. (2022). Catalytic nitrogen fixation using visible light energy. Nat. Commun. *13*, 7263. https://doi.org/10.1038/s41467-022-34984-1.
6. Li, S., Medrano Jimenez, J., Hessel, V., and Gallucci, F. (2018). Recent progress of plasma-assisted nitrogen fixation research: a review. Processes *6*, 248. https://doi.org/10.3390/pr6120248.
7. Vervloessem, E., Aghaei, M., Jardali, F., Hafezkhiabani, N., and Bogaerts, A. (2020). Plasma-based N_2 fixation into NOx: insights from modeling toward optimum yields and energy costs in a gliding arc plasmatron. ACS Sustain. Chem. Eng. *8*, 9711–9720. https://doi.org/10.1021/acssuschemeng.0c01815.
8. Ye, T.N., Park, S.W., Lu, Y., Li, J., Sasase, M., Kitano, M., Tada, T., and Hosono, H. (2020). Vacancy-enabled N_2 activation for ammonia synthesis on an Ni-loaded catalyst. Nature *583*, 391–395. https://doi.org/10.1038/s41586-020-2464-9.
9. Foster, S.L., Bakovic, S.I.P., Duda, R.D., Maheshwari, S., Milton, R.D., Minteer, S.D., Janik, M.J., Renner, J.N., and Greenlee, L.F. (2018). Catalysts for nitrogen reduction to ammonia. Nat. Catal. *1*, 490–500. https://doi.org/10.1038/s41929-018-0092-7.
10. Hollevoet, L., Jardali, F., Gorbanev, Y., Creel, J., Bogaerts, A., and Martens, J.A. (2020). Towards green ammonia synthesis through plasma-driven nitrogen oxidation and catalytic reduction. Angew. Chem. Int. Ed. *59*, 23825–23829. https://doi.org/10.1002/anie.202011676.
11. Han, K., Luo, J., Feng, Y., Lai, Q., Bai, Y., Tang, W., and Wang, Z.L. (2020). Wind-driven radial-engine-shaped triboelectric nanogenerators for self-powered absorption and degradation of NOx. ACS Nano *14*, 2751–2759. https://doi.org/10.1021/acsnano.9b08496.
12. Pang, Y., Cao, Y., Derakhshani, M., Fang, Y., Wang, Z.L., and Cao, C. (2021). Hybrid energy-harvesting systems based on triboelectric nanogenerators. Matter *4*, 116–143. https://doi.org/10.1016/j.matt.2020.10.018.
13. Zi, Y., Guo, H., Wen, Z., Yeh, M.H., Hu, C., and Wang, Z.L. (2016). Harvesting low-frequency (<5 Hz) irregular mechanical energy: a possible killer application of triboelectric nanogenerator. ACS Nano *10*, 4797–4805. https://doi.org/10.1021/acsnano.6b01569.
14. Liu, L., Zhou, L., Liu, D., Yuan, W., Chen, S., Li, H., Bian, Z., Wang, J., and Wang, Z.L. (2021). Improved degradation efficiency of levofloxacin by a self-powered electrochemical system with pulsed direct-current. ACS Nano *15*, 5478–5485. https://doi.org/10.1021/acsnano.1c00233.
15. Han, K., Luo, J., Feng, Y., Xu, L., Tang, W., and Wang, Z.L. (2020). Self-powered electrocatalytic ammonia synthesis directly from air as driven by dual triboelectric nanogenerators. Energy Environ. Sci. *13*, 2450–2458. https://doi.org/10.1039/d0ee01102a.
16. Han, K., Luo, J., Chen, J., Chen, B., Xu, L., Feng, Y., Tang, W., and Wang, Z.L. (2021). Self-powered ammonia synthesis under ambient conditions via N_2 discharge driven by Tesla turbine triboelectric nanogenerators. Microsyst. Nanoeng. *7*, 7. https://doi.org/10.1038/s41378-020-00235-w.
17. Gao, S., Zhu, Y., Chen, Y., Tian, M., Yang, Y., Jiang, T., and Wang, Z.L. (2019). Self-power electroreduction of N_2 into NH_3 by 3D printed triboelectric nanogenerators. Mater. Today *28*, 17–24. https://doi.org/10.1016/j.mattod.2019.05.004.
18. Cheng, J., Ding, W., Zi, Y., Lu, Y., Ji, L., Liu, F., Wu, C., and Wang, Z.L. (2018). Triboelectric microplasma powered by mechanical stimuli. Nat. Commun. *9*, 3733. https://doi.org/10.1038/s41467-018-06198-x.
19. Li, S., Zhang, B., Gu, G., Fang, D., Xiang, X., Zhang, W., Zhu, Y., Wang, J., Cuo, J., Cui, P., et al. (2022). Triboelectric plasma CO_2 reduction reaching a mechanical energy conversion efficiency of 2.3%. Adv. Sci. *9*, e2201633. https://doi.org/10.1002/advs.202201633.
20. Ren, Y., Yu, C., Wang, L., Tan, X., Wang, Z., Wei, Q., Zhang, Y., and Qiu, J. (2022). Microscopic-level insights into the mechanism of enhanced NH_3 synthesis in plasma-enabled cascade N_2 oxidation-electroreduction system. J. Am. Chem. Soc. *144*, 10193–10200. https://doi.org/10.1021/jacs.2c00089.
21. Hojnik, N., Modic, M., Ni, Y., Filipič, G., Cvelbar, U., and Walsh, J.L. (2019). Effective fungal spore inactivation with an environmentally friendly approach based on atmospheric pressure air plasma. Environ. Sci. Technol. *53*, 1893–1904. https://doi.org/10.1021/acs.est.8b05386.
22. Chen, J., Cheng, G., Liu, R., Zheng, Y., Huang, M., Yi, Y., Shi, X., Du, Y., and Deng, H. (2018). Managing and maximizing the output power of a triboelectric nanogenerator by controlled tip-electrode air-discharging and application for UV sensing. Nano Energy *523*, 208–216. https://doi.org/10.1016/j.nanoen.2017.11.062.
23. Li, S., Zhang, B., Gu, G., Xiang, X., Zhang, W., Shi, X., Zhao, K., Zhu, Y., Guo, J., Cui, P., et al. (2021). Triboelectric plasma decomposition of CO_2 at room temperature driven by mechanical energy. Nano Energy *88*, 106287. https://doi.org/10.1016/j.nanoen.2021.106287.
24. Wong, M.C., Xu, W., and Hao, J. (2019). Microplasma-discharge-based nitrogen fixation driven by triboelectric nanogenerator toward self-powered mechano-nitrogenous fertilizer supplier. Adv. Funct. Mater. *29*, 1904090. https://doi.org/10.1002/adfm.201904090.
25. Britun, N., Gamaleev, V., and Hori, M. (2021). Evidence of near-the-limit energy cost NO formation in atmospheric spark discharge. Plasma Sources Sci. Technol. *30*, 08LT02. https://doi.org/10.1088/1361-6595/ac12bf.
26. Janda, M., Morvova, M., Machala, Z., and Morva, I. (2008). Study of plasma induced chemistry by DC discharges in $CO_2/N_2/H_2O$ mixtures above a water surface. Orig. Life Evol. Biosph. *38*, 23–35. https://doi.org/10.1007/s11084-007-9115-0.
27. Feng, Y., Zhang, L., Zheng, Y., Wang, D., Zhou, F., and Liu, W. (2019). Leaves based triboelectric nanogenerator (TENG) and TENG tree for wind energy harvesting. Nano Energy *55*, 260–268. https://doi.org/10.1016/j.nanoen.2018.10.075.
28. Winter, L.R., and Chen, J.G. (2021). N_2 fixation by plasma-activated processes. Joule *5*,

300–315. https://doi.org/10.1016/j.joule.2020.11.009.

29. Pei, X., Gidon, D., Yang, Y.J., Xiong, Z., and Graves, D.B. (2019). Reducing energy cost of NOx production in air plasmas. Chem. Eng. J. *362*, 217–228. https://doi.org/10.1016/j.cej.2019.01.011.

30. Jardali, F., Van Alphen, S., Creel, J., Ahmadi Eshtehardi, H., Axelsson, M., Ingels, R., Snyders, R., and Bogaerts, A. (2021). NOx production in a rotating gliding arc plasma: potential avenue for sustainable nitrogen fixation. Green Chem. *23*, 1748–1757. https://doi.org/10.1039/d0gc03521a.

31. Patil, B.S., Wang, Q., Hessel, V., and Lang, J. (2015). Plasma N_2-fixation: 1900-2014. Catal. Today *256*, 49–66. https://doi.org/10.1016/j.cattod.2015.05.005.

32. Janda, M., Martišovitš, V., Hensel, K., and Machala, Z. (2016). Generation of antimicrobial NOx by atmospheric air transient spark discharge. Plasma Chem. Plasma Process. *36*, 767–781. https://doi.org/10.1007/s11090-016-9694-5.

33. Rahman, M., and Cooray, V. (2003). NOx generation in laser-produced plasma in air as a function of dissipated energy. Opt Laser. Technol. *35*, 543–546. https://doi.org/10.1016/S0030-3992(03)00077-X.

34. Wang, W., Patil, B., Heijkers, S., Hessel, V., and Bogaerts, A. (2017). Nitrogen fixation by gliding arc plasma: better insight by chemical kinetics modelling. ChemSusChem *10*, 2145–2157. https://doi.org/10.1002/cssc.201700095.

35. Rehbein, N., and Cooray, V. (2001). NOx production in spark and corona discharges. J. Electrostat. *51-52*, 333–339. https://doi.org/10.1016/S0304-3886(01)00115-2.

36. Pavlovich, M.J., Ono, T., Galleher, C., Curtis, B., Clark, D.S., Machala, Z., and Graves, D.B. (2014). Air spark-like plasma source for antimicrobial NOx generation. J. Phys. D Appl. Phys. *47*, 505202. https://doi.org/10.1088/0022-3727/47/50/505202.

37. Bian, W., Shi, J., and Yin, X. (2009). Nitrogen fixation into water by pulsed high-voltage discharge. IEEE Trans. Plasma Sci. *37*, 211–218. https://doi.org/10.1109/Tps.2008.2007585.

38. Pei, X., Gidon, D., and Graves, D.B. (2020). Specific energy cost for nitrogen fixation as NOx using DC glow discharge in air. J. Phys. D Appl. Phys. *53*, 044002. https://doi.org/10.1088/1361-6463/ab5095.

39. Vervloessem, E., Gorbanev, Y., Nikiforov, A., De Geyter, N., and Bogaerts, A. (2022). Sustainable NOx production from air in pulsed plasma: elucidating the chemistry behind the low energy consumption. Green Chem. *24*, 916–929. https://doi.org/10.1039/d1gc02762j.

40. Ma, H., Sharma, R.K., Welzel, S., van de Sanden, M.C.M., Tsampas, M.N., and Schneider, W.F. (2022). Observation and rationalization of nitrogen oxidation enabled only by coupled plasma and catalyst. Nat. Commun. *13*, 402. https://doi.org/10.1038/s41467-021-27912-2.

41. Bogaerts, A., and Neyts, E.C. (2018). Plasma technology: an emerging technology for energy storage. ACS Energy Lett. *3*, 1013–1027. https://doi.org/10.1021/acsenergylett.8b00184.

42. Shan, C., Liu, W., Wang, Z., Pu, X., He, W., Tang, Q., Fu, S., Li, G., Long, L., Guo, H., et al. (2021). An inverting TENG to realize the AC mode based on the coupling of triboelectrification and air-breakdown. Energy Environ. Sci. *14*, 5395–5405. https://doi.org/10.1039/d1ee01641e.

43. Rouwenhorst, K.H.R., Jardali, F., Bogaerts, A., and Lefferts, L. (2021). From the Birkeland-Eyde process towards energy-efficient plasma-based NO_X synthesis: a techno-economic analysis. Energy Environ. Sci. *14*, 2520–2534. https://doi.org/10.1039/d0ee03763j.

44. Mehta, P., Barboun, P., Go, D.B., Hicks, J.C., and Schneider, W.F. (2019). Catalysis enabled by plasma activation of strong chemical bonds: a review. ACS Energy Lett. *4*, 1115–1133. https://doi.org/10.1021/acsenergylett.9b00263.

45. Schlögl, R. (2003). Catalytic synthesis of ammonia-a "never-ending story. Angew. Chem. Int. Ed. *42*, 2004–2008. https://doi.org/10.1002/anie.200301553.

46. Meng, S.L., Li, X.B., Tung, C.H., and Wu, L.Z. (2021). Nitrogenase inspired artificial photosynthetic nitrogen fixation. Chem *7*, 1431–1450. https://doi.org/10.1016/j.chempr.2020.11.002.

47. Medford, A.J., and Hatzell, M.C. (2017). Photon-driven nitrogen fixation: current progress, thermodynamic considerations, and future outlook. ACS Catal. *7*, 2624–2643. https://doi.org/10.1021/acscatal.7b00439.

48. Shiraishi, Y., Chishiro, K., Tanaka, S., and Hirai, T. (2020). Photocatalytic dinitrogen reduction with water on boron-doped carbon nitride loaded with nickel phosphide particles. Langmuir *36*, 734–741. https://doi.org/10.1021/acs.langmuir.9b03445.

49. Xiao, C., Hu, H., Zhang, X., and MacFarlane, D.R. (2017). Nanostructured gold/bismutite hybrid heterocatalysts for plasmon-enhanced photosynthesis of ammonia. ACS Sustainable Chem. Eng. *5*, 10858–10863. https://doi.org/10.1021/acssuschemeng.7b02788.

50. Niu, S., Liu, Y., Chen, X., Wang, S., Zhou, Y.S., Lin, L., Xie, Y., and Wang, Z.L. (2015). Theory of freestanding triboelectric-layer-based nanogenerators. Nano Energy *12*, 760–774. https://doi.org/10.1016/j.nanoen.2015.01.013.

51. Zhu, Y., Chen, X., Wu, Y., Hao, J., Ma, X., Lu, P., and Tardiveau, P. (2021). Simulation of ionization-wave discharges: a direct comparison between the fluid model and E-FISH measurements. Plasma Sources Sci. Technol. *30*, 075025. https://doi.org/10.1088/1361-6595/ac0714.

52. Zhu, Y., and Starikovskaia, S. (2018). Fast gas heating of nanosecond pulsed surface dielectric barrier discharge: spatial distribution and fractional contribution from kinetics. Plasma Sources Sci. Technol. *27*, 124007. https://doi.org/10.1088/1361-6595/aaf40d.